Research Article | Vol. 9, No. 11 | 1 Nov 2018 | BIOMEDICAL OPTICS EXPRESS 5115
Biomedical Optics EXPRESS

Holmium:yttrium-aluminum-garnet laser induced lithotripsy: in-vitro investigations on fragmentation, dusting, propulsion and fluorescence

Maximilian Eisel,[1,2,*] Stephan Ströbl,[1,2] Thomas Pongratz,[1,2] Frank Strittmatter,[2] and Ronald Sroka[1,2]

[1]*Laser-Forschungslabor, LIFE-Zentrum, University Hospital of Munich, Munich, Germany*
[2]*Department of Urology, University Hospital of Munich, Munich, Germany*
**Max.Eisel@med.uni-muenchen.de*

Abstract: The fragmentation efficiency on Bego artificial stones during lithotripsy and the propulsive effect (via video tracking) was investigated for a variety of laser settings. A variation of the laser settings (pulse energy, pulse duration, repetition rate) altered the total application time required for stone fragmentation, the stone break up time, and the propulsion. The obtained results can be used to develop lithotripsy devices providing an optimal combination of low stone propulsion and high fragmentation efficacy, which can then be evaluated in a clinical setting. Additionally, the fluorescence of human kidney stones was inspected endoscopically in vivo. Fluorescence light can be used to detect stone-free areas or to clearly distinguish calculi from surrounding tissue or operation tools.

© 2018 Optical Society of America under the terms of the OSA Open Access Publishing Agreement

1. Introduction

Ureteroscopic Ho:YAG laser lithotripsy is a preferred method for treating urinary stone disease [1–6]. Clinical lithotripsy is performed endoscopically by application of laser pulses to the calculi. The laser light is guided to the stone by an optical wave guide that is inserted into the working channel of either a rigid or flexible endoscope. Clinically, Ho:YAG lasers (λ = 2.1 µm) are widely used for this application, owing to the high absorption coefficient of water at the respective wavelength. This allows to induce not only thermo-mechanical ablation on the stone surface, but also photothermal fragmentation by expansion of the water contained in urinary stones [7]. To compare different laser systems and laser parameters, different experimental set-ups have been proposed [8–14]. Such set-ups were designed to quantify the fragmentation rate and the dusting efficacy. Although the term dust has not been defined finally to distinguish between the two processes, a definition of dust as fragments smaller than 1 mm has been proposed [15]. Along with the desired stone destruction, pulsed laser light also accelerates the urinary stone (propulsion effect), resulting in the need to "chase the stone" with the endoscope along the ureter. Such manoeuvres may result in a longer treatment time and the possibility of losing the stone or stone fragments [9, 10, 16]. Both, fragmentation and propulsion processes, are highly influenced by the chosen laser parameters (pulse energy, pulse duration, repetition rate) [15, 17, 18]. The propulsion can be measured via a variety of methods, for example by evaluating the maximum deflection angle of a pendulum due to laser impact [18–21] or by analysing horizontal [9–12] or vertical stone movements [13] in terms of maximum stone displacement. The main disadvantage of these techniques is that the propulsion effect of only one single laser pulse can be evaluated. In this study, a combination of maximum vertical stone displacement analysis and object tracking via high speed camera was used to determine the propulsion characteristics of pulse trains over an observation time of 7 seconds [22]. Beyond the quantification of stone destruction and propulsion, a third challenge is posed by the proper detection of small fragments. Small fragments may remain untreated clinically because of insufficient visibility and/or low

#335764 https://doi.org/10.1364/BOE.9.005115
Journal © 2018 Received 21 Jun 2018; revised 16 Aug 2018; accepted 1 Sep 2018; published 2 Oct 2018

Biomedical Optics EXPRESS

contrast with the surrounding tissue under white light illumination. Suitable recognition techniques have been proposed and are still under development [23–25]. In view of these three clinical challenges, the following investigations on fragmentation and propulsion of artificial stones as well as fluorescence response of human calculi were performed to identify optimisation potential in the procedure of laser lithotripsy. The main focus was set on the fragmentation and propulsion experiments using an experimental laser system, while for fluorescence response measurements first results are shown.

2. Material and methods

2.1 Laser device and artificial calculi

As laser source an experimental Ho:YAG device (λ = 2.1 µm) was used, providing a huge range of laser settings: pulse energies (E) from 0.5 J/pulse up to 2.5 J/pulse, repetition rates (f) from 10 Hz to 80 Hz, and optical pulse durations (t) up to 4 ms. A detailed listing of the settings used is shown in Table 1. One combined setting was used where the stone was fragmented until the stone broke up (t_{break}) with 0.5 J/pulse, 0.4 ms pulse length and 80 Hz repetition rate, then the fragmentation was continued using 2.5 J/pulse, 4.0 ms and 10 Hz. As the used laser source was an experimental device it was decided to use an optical fiber with core diameter of 365 µm for all experiments to guarantee optimal coupling efficacy and to prevent damage to the coupling optics, the coupling plug or the fiber itself. With the laser device it was possible to create a great variation in pulse length (0.25 ms- 4.0 ms), energy per pulse (0.4 J/pulse - 2.5 J/pulse). Depending on the pulse length and energy per pulse repetition rates up to 80 Hz could be used. The selection of settings in Table 1 was chosen due to experiences from former experiments [15, 20, 22, 26] with standard Ho:YAG laser sources and current state of the art laser settings using high repetition rates in combination with variations in pulse length and energy per pulse [13, 27, 28].

Table 1. Laser settings used for fragmentation and propulsion experiments

E [J]	t [ms]	f [Hz]	$P_{Average}$ [W]
0.5	0.3	10	5
0.5	0.4	80	40
0.5	0.6	10	5
0.5	1.0	10	5
0.5	1.2	40	20
0.5	1.3	10	5
0.5	1.6	10	5
0.5	2.2	30	15
1.0	0.3	10	10
1.0	0.6	10	10
1.0	1.0	10	10
1.0	1.2	10	10
1.0	0.8	40	32
1.0	1.2	40	40
1.0	1.6	10	10
1.0	2.2	30	30
1.5	0.3	10	15
1.5	1.0	10	15
2.0	0.3	10	20
2.0	1.0	10	20
2.0	4.0	10	20
2.5	4.0	10	25

Cubical (edge length: 5 mm) and spherical (Ø: 6 mm) artificial calculi made out of Bego powder (BEGO, BEGO GmbH & Co KG, Bremen, Germany) were used for the fragmentation and propulsion experiments. All stones were used “dry” without immersion in water beforehand. The hardness of the calculi was adjusted by the compound-to-water ratio

Biomedical Optics EXPRESS

(here: 15:4) and comparable to human kidney stones, for a composition intermediate between calcium oxalate monohydrate and ammonium magnesium phosphate hydrate [29].

2.2 Fragmentation set-up

Laser light delivered via a standard optical fibre ($Ø_{core}$: 365µm) was directed perpendicularly from the top onto the surface of artificial calculi recumbent in an acrylic glass vessel that was submerged in water (Fig. 1). An adjustable water flow (max. 250 ml/min) provided for clear vision even if the used laser setting produced a lot of dust. By moving the application fiber smoothly across the surface of the stone phantom, thereby maintaining mechanical contact, the stone was ablated layer by layer until the vessel was free from any stone debris.

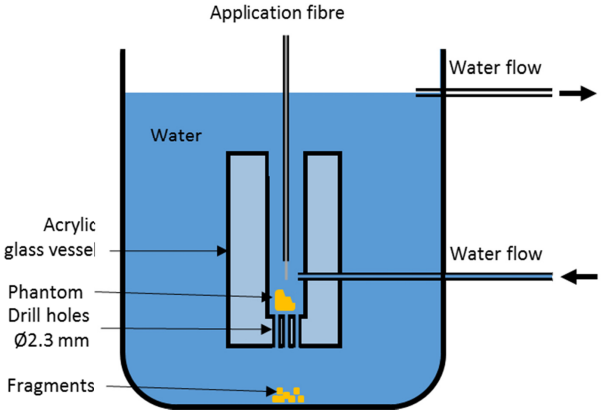

Fig. 1. Experimental set-up for the investigation of fragmentation and dusting efficacy.

The total application time (t_{total}) was defined as the period it took to destruct the stone until all fragments were smaller than 2.3 mm [30] and hence had fallen through the holes drilled into the bottom of the vessel. Additionally, the "break up" time (t_{break}) was recorded, defined as the application time after which the stone broke up for the first time, marking the cross-over from pure dusting to combined fragmentation and dusting. The time after break ($t_{afterbreak}$) was defined as the remaining time, calculated according to E1 of Table 2. Weighing of each single artificial calculus was performed prior to each experiment. After each experiment and after sieving and drying of the residual fragments (defined by a fragment size between 1 mm and 2.3 mm), the fragments were weighed (MC1, SartoriusAG, Göttingen, Germany). The amount of dust (m_{dust}) produced could then be calculated by taking the difference between the initial mass ($m_{initial}$) and the residual fragments' mass ($m_{fragment}$) (E2). The dusting ratio $D = m_{dust}/m_{initial}$ was used as a quantitative measure of the dusting efficacy (E3). All experiments were performed several times ($n \geq 5$) for each set of laser parameters (pulse energy, pulse duration, repetition rate) according to Table 1.

Table 2. Evaluation of the fragmentation experiment.

E1	Total application time t_{total}	$t_{afterbreak} = t_{total} - t_{break}$
E2	Mass of dust m_{dust}	$m_{dust} = m_{initial} - m_{fragment}$
E3	Dust ratio D	$D = m_{dust}/m_{initial} \cdot 100\%$

2.3 Propulsion set-up

As shown in Fig. 2, a user-independent experiment set-up was created in which the pulsed laser light was applied from below to cubical and spherical BegoStone phantoms loosely guided within a vertical column filled with water. The stone movement was recorded via a high speed camera system with 1000 fps (DSC RX-100 V, Sony, Tokyo, Japan). The total recording time was limited to 7 seconds by the internal buffer space, hence just 7 second long movement profiles could be evaluated.

Biomedical Optics EXPRESS

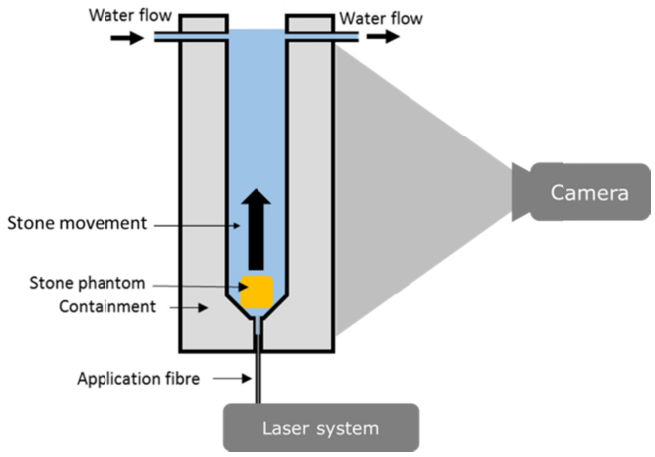

Fig. 2. Experimental set-up for the propulsion measurement.

These movement profiles were generated by a video tracking method [22] that uses an automatic algorithm to determine the vertical stone position (centroid amplitude) in each frame of a recorded scene. Two exemplary movement profiles are shown in Fig. 3 for a cubical and a spherical artificial stone. The time-dependence of the vertical stone position is characterized by an irregular series of peaks. By analysing the slopes of the rising flanks of these peaks it was possible to determine the mean upward velocity of the stone for a whole pulse train scene of up to 7 s duration and finally to use this for comparison of the propulsion effects associated with different laser settings.

The water flow was set constant (150 ml/min) and provided for clear vision into the vessel under consistent conditions (regarding water level and flow) for every single experiment on cubical and spherical artificial stones. A repetition rate of 10 Hz was chosen for all experiments, while pulse energies were varied from 0.5 J/pulse to 2.0 J/pulse in 0.5 J/pulse steps and pulse durations from 0.3 ms to 1.0 ms according to Table 1. For each laser setting, the experiment was repeated on n = 15 different freshly prepared stones. The mean value out of these 15 measurements was used to estimate the propulsion effect for each laser setting.

Biomedical Optics EXPRESS

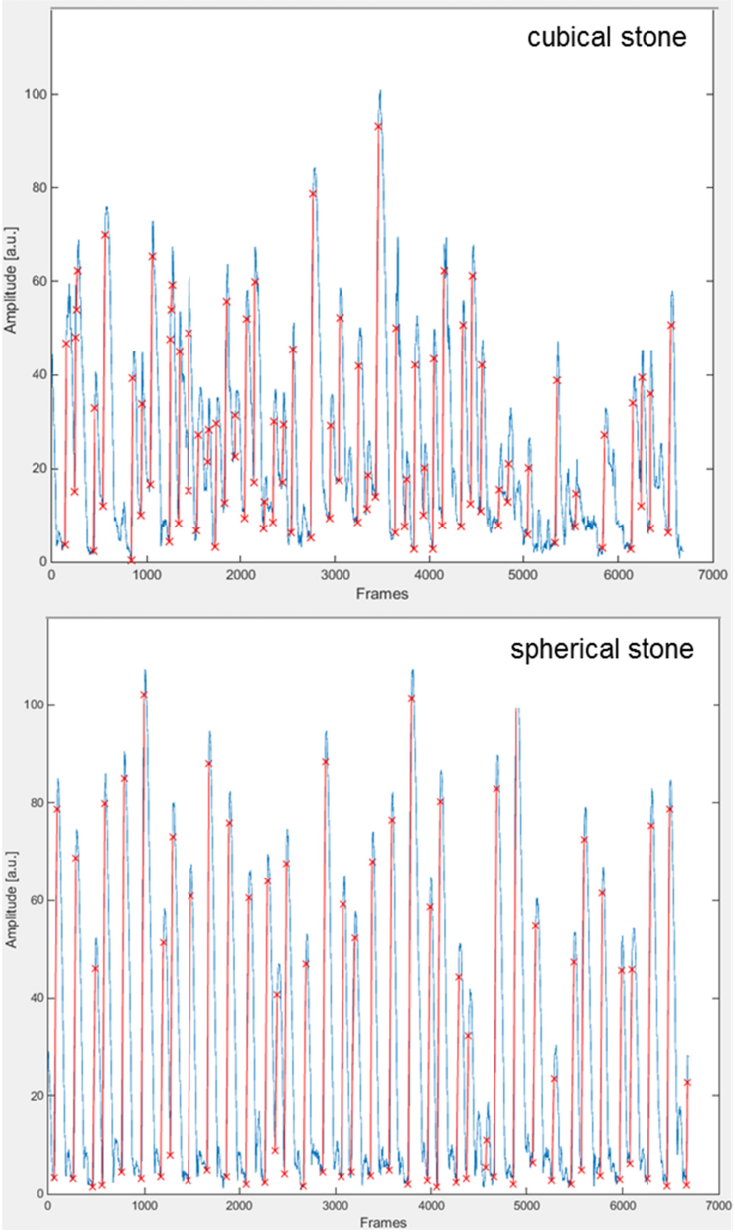

Fig. 3. Vertical centroid coordinate of a cubical (upper graph) and a spherical (lower graph) phantom stone observed during laser application (1 J/pulse, 1 ms, 10 Hz) as a function of the frame number.

2.4 Fluorescence measurement

Urinary stones harvested from patients were spectrally analyzed in in-vitro measurements via a fluorescence microscope (Leica DM IRBE, Wetzlar, Germany) under illumination with light from a bandpass filtered mercury arc lamp (Osram HBO 103, Munich, Germany) as shown in Fig. 4. Images were taken with an attached camera system (telcam SL pal 20212020, KARL STORZ GmbH & Co. KG, Tuttlingen, Germany), while a spectrometer (USB 2000 + , Ocean Optics, Ostfildern, Germany) recorded the spectral data from a small spot in the center of the image (Fig. 4).

Biomedical Optics EXPRESS

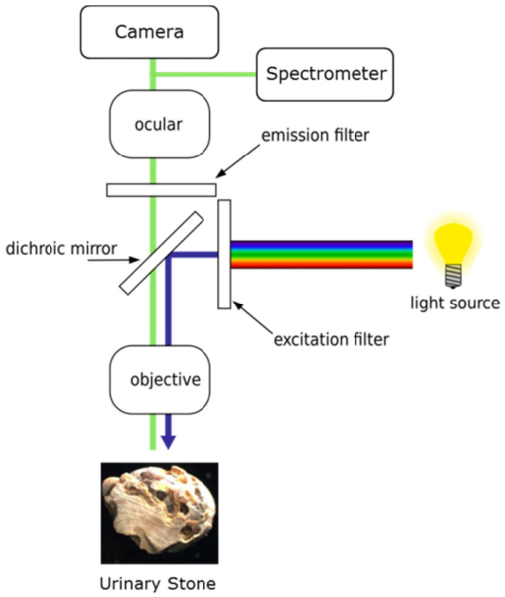

Fig. 4. Schematic set-up of fluorescence microscope.

Using different excitation filters, light of the wavelength bands (400 ± 5) nm, (450 ± 10) nm and (550 ± 5) nm was applied to the stone (30% calcium-oxalate-monohydrate, 70% carbonate apatite) for fluorescence excitation. The thereupon emitted fluorescence light was detected after passing long pass filters of $\lambda > 470$ nm, $\lambda > 520$ nm and $\lambda > 590$ nm, respectively.

Additionally, the fluorescence of two urinary stones (stone 1: 100% calcium-oxalate-monohydrate; stone 2: 80% uric acid, 20% calcium-oxalate-monohydrate) was inspected in-vivo during endoscopic stone treatments to identify potential advantages of fluorescence guidance during this procedure. In this case, the endoscopic scene was illuminated first with white light and subsequently with green light (λ = 500-570 nm, Light source: D-Light C 20133220, Karl-Storz SE & Co. KG, Tuttlingen, Germany; Band pass filter: 540/60, transmission >80% in the range 500-567 nm, AHF Analysetechnik, Tübingen, Germany). The stone fluorescence was observed through a long pass filter ($\lambda > 610$ nm) via the ocular of the endoscope. White light and fluorescence response images were subjectively compared to each other.

2.5 Statistical evaluation

Statistical evaluation of the data (mean, standard deviation, significance) was performed using Sigma Plot (V.11.0, Systat Software GmbH, Erkrath, Germany). To test the significance of differences between the obtained means for multiple groups, the one way ANOVA (Holm-Sidak) method was used.

3. Results

3.1 Fragmentation

In Fig. 5 and Fig. 6 selected results of the experiments regarding t_{total}, t_{break}, and $t_{afterbreak}$ are shown. Figure 5 presents all settings with average powers 10 W (upper section) and 5 W (lower section) using pulse length from 0.3 ms up to 1.6 ms. The amount of dust produced ranged between around 60% (1.0J/pulse, 0.3 ms, 10 Hz) and 73% (1J/pulse, 1.2 ms, 10 Hz). Concerning t_{break} all settings showed significant difference ($p<0.001$), except for the two 5W settings (with 1.3 ms and 1.6 ms optical pulse length) ($p = 0.056$). Regarding the total

Biomedical Optics EXPRESS

application time t_{total} the 10W situations showed just significant difference for pulse length of 0.3 ms and 1.2 ms, while all 5 W settings were significant different.

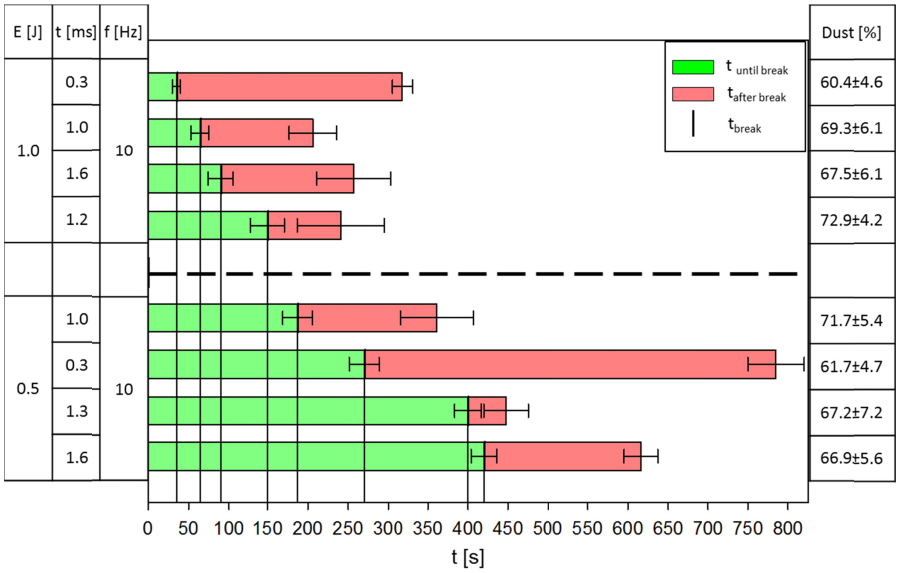

Fig. 5. Fragmentation times and dusting ratios for varying pulse duration, obtained at a constant repetition rate of 10 Hz for pulse energies of 1.0 J ($P_{Average}$: 10W, upper section) and 0.5 J ($P_{Average}$: 10W, lower section), respectively. Different optical pulse lengths (0.3ms-1.6ms) were investigated. Error bars represent the standard deviations of the total application time t_{total} and the break up time t_{break}. The dusting ratios with their respective standard deviation are shown in the right column.

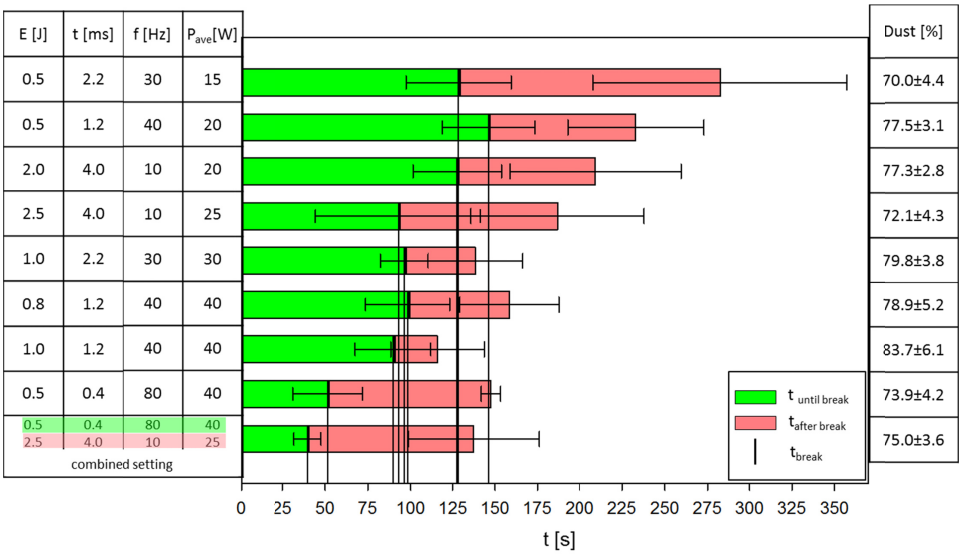

Fig. 6. Fragmentation times and dusting ratios for a selection of pulse energies, pulse durations, and repetitions rates sorted by the average power of each setting. Error bars represent the standard deviations of the total application time t_{total} and the break up time t_{break}. In case of the combined setting the laser configuration (0.5J/pulse, 0.4 ms, 80 Hz) for treatment until t_{break} is highlighted in green and the setting for further fragmentation (2.5J/pulse, 4.0 ms, 10 Hz) in red. The dusting ratios with their respective standard deviation are shown in the right column.

Biomedical Optics EXPRESS

In Fig. 6 the fragmentation experiment results for settings from average power of 15 W up to 40 W are illustrated. The highest application time t_{total} was around 280s, the shortest time measured roughly 115 s. Dusting ratios were ranging between 70% (setting 1: 0.5J/pulse, 2.2 ms, 30 Hz) up to nearly 84% (setting 7: 1.0 J/pulse, 1.2 ms, 40 Hz). The four fastest settings concerning t_{total} were (setting 5: 1.0J/pulse, 2.2 ms, 30 Hz), setting 7 (setting 8: 0.5J/pulse, 0.4 ms, 80 Hz) and (setting 9: setting 8 + 4). No significant difference ($p<0.001$) could be found concerning the total application time, for t_{break} there were significant differences except for setting combinations of 5 and 7 ($p = 0.597$) as well as for 8 and 9 ($p = 0.593$). Doubling the energy per pulse from 0.5 J for setting 1 (0.5J/pulse, 2.2 ms, 30 Hz) to 1.0 J in setting 5 (1.0J/pulse, 2.2 ms, 30 Hz) showed significant difference in t_{total} but not in $t_{break.}$ Comparing the two 40 Hz settings 2 (0.5 J/pulse, 1.2 ms, 40 Hz) and 7 (1.0 J/pulse, 1.2 ms, 40 Hz) there was significant difference for t_{total} and t_{break}. All in all the fragmentation of stones using a variety of laser settings showed a great variation in total application time from around 120 s (1.0 J, 1.2 ms, 40 Hz) (Fig. 6) to almost 800 s (0.5 J, 0.3 ms, 10 Hz) (Fig. 5). Apparently, based on the selection of laser settings in Fig. 5, a pulse energy of at least 1.0 J is recommendable for efficient fragmentation in terms of total application time. In combination with high repetition rates (80 Hz), however, low pulse energy settings (0.5 J, 0.4 ms, 80 Hz) may also lead to fairly fast fragmentation (Fig. 6).

3.2 Propulsion

In Fig. 7 the evaluated average vertical velocity values are displayed for a selection of 9 different laser settings, in each case for both, the cubical and the spherical phantom model. The propulsive effect, respectively the mean upward velocity of the stone, increases with increasing pulse energy only very slightly, whereas an elongation of the pulse duration is clearly associated with a declining mean upward velocity. As the repetition rate remained unchanged at 10 Hz in all experiments, it is not possible to make a statement about a potential influence of the repetition rate on the propulsive effect.

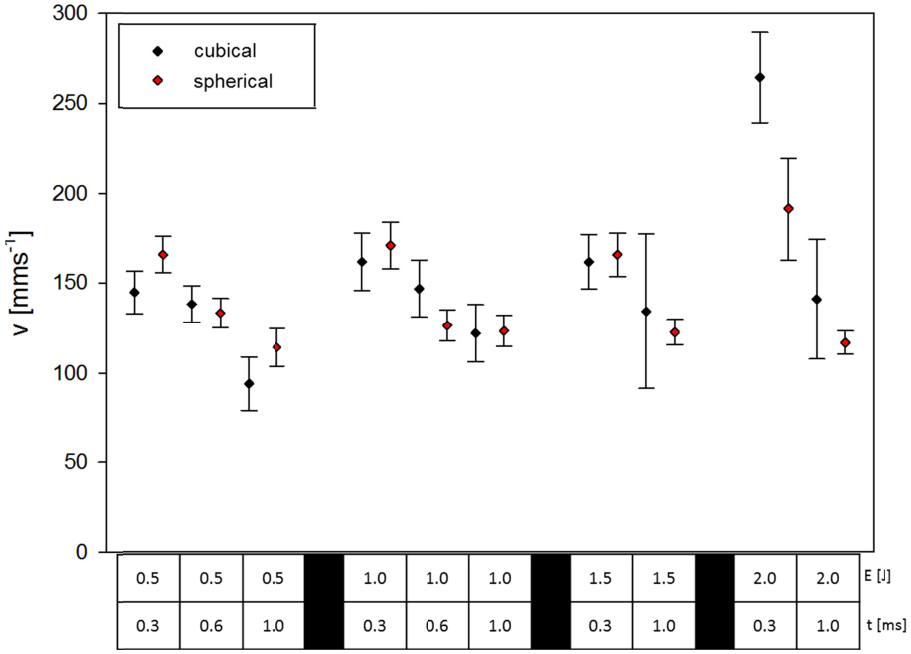

Fig. 7. Comparison of laser-induced stone phantom propulsion velocities v obtained with the video tracking software at a constant repetition rate of 10 Hz for different pulse energies E (0.5J-2J), respectively average powers P_{Ave} (5W-20W) and pulse durations t. The data points and error bars represent the mean propulsion velocities and their standard deviations.

Biomedical Optics EXPRESS

3.3 Fluorescence

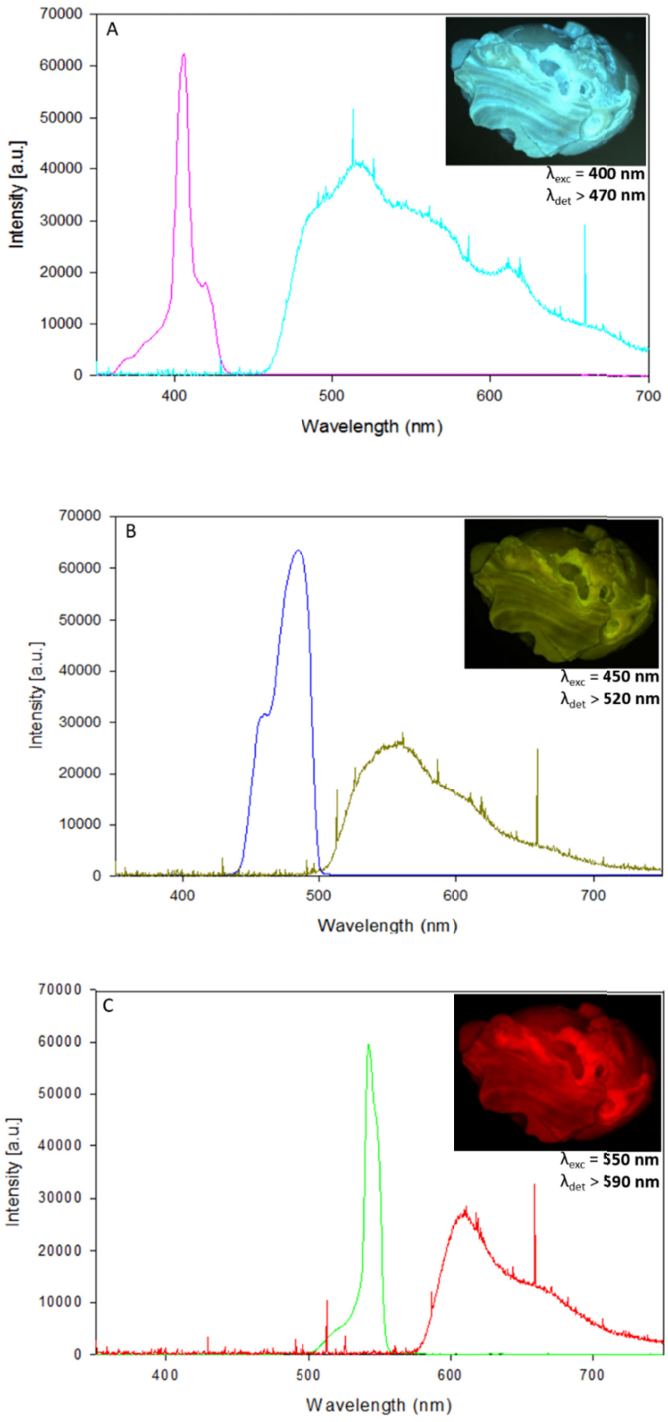

Fig. 8. Fluorescence response of a human kidney stone (Inset) using three different excitation wavelengths (λ_{exc}: 400 nm, 450 nm, 550 nm) and corresponding long pass emission filters (λ_{onset}: 470 nm, 520 nm, 590 nm).

Biomedical Optics EXPRESS

In Fig. 8 exemplary fluorescence emission spectra are shown, obtained in vitro from a human kidney stone for three different excitation wavelengths (λ_{exc}: 400 nm, 450 nm, 550 nm). The graphs illustrate that the stones exhibit a well detectable amount of fluorescence emission, covering a broad spectral range from 580 nm to 740 nm when excited with 550 nm and detected through a long pass filter with a nominal onset wavelength of 590 nm.

Endoscopic white light and fluorescence images of urinary stones obtained in a clinical situation under white light and green light illumination (λ_{exc}: 500-570 nm, λ_{det}: >610 nm), respectively, are shown in Fig. 9. Under white light illumination the stone can hardly be distinguished from surrounding tissue and catheters, under green light illumination the boundaries between stone and tissue are clearly visible. Due to the emitted fluorescence, stone 1 shows an enhancement in contrast. Stone 2 is already clearly distinguishable from the surrounding tissue under white light illumination. Endoscopic devices (e.g. catheter, guide wire, marked by red cycles in Fig. 9) are not visible at all in the case of fluorescence detection under green light illumination as they do not show any fluorescence under these conditions.

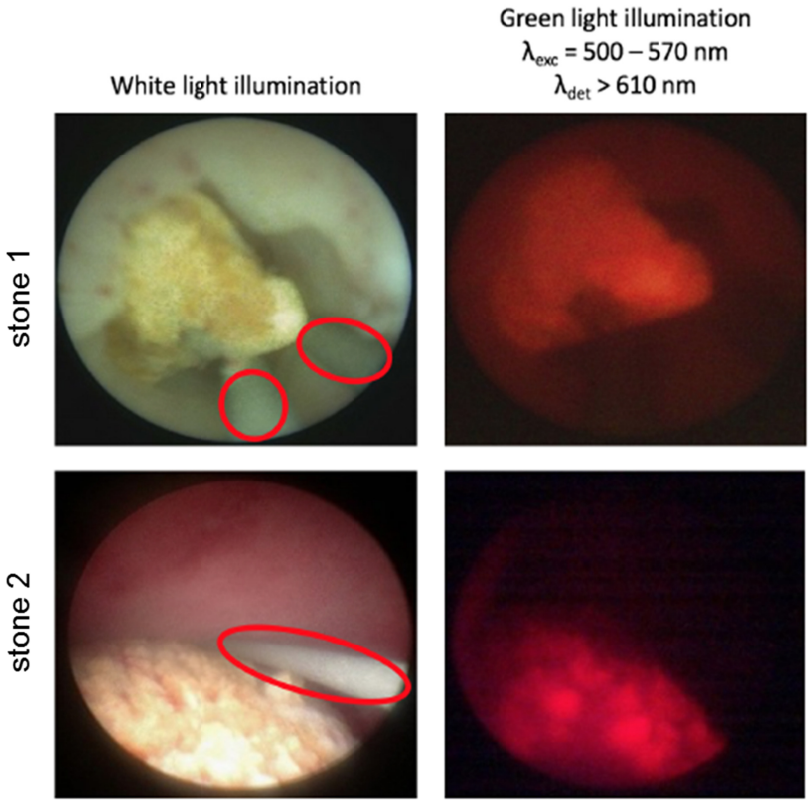

Fig. 9. White light and fluorescence images of two urinary stones recorded in vivo with an endoscopic camera system. For fluorescence excitation, filtered green light illumination (λ_{exc} = 500 – 570 nm) was applied, for fluorescence detection, a long-pass filter (λ_{det} > 610nm) was implemented in the imaging system. Endoscopic tools are highlighted with red circles.

4. Discussion

Our examination of stone fragmentation using a selection of different laser settings showed that varying the laser parameters (pulse energy, pulse duration, repetition rate) altered the total application time as well as the break up time. In this context the propulsion, even if not measured for all settings, appears to be higher for shorter pulse duration (for constant pulse energy and repetition rate) and may also have an additional effect on the fragmentation due to

Biomedical Optics EXPRESS

time consuming chasing of the fragments respectively the break-up behaviour. For time-effective fragmentation it would be desirable to have maximal ablation rate (total application time short) with late break-up of the treated stone (fragments occur very late during the application) and low propulsion when it comes to "chasing" the remaining fragments. Generally speaking, a simultaneous increase of pulse energy and/or pulse duration as well as using repetition rates above 30 Hz seems to be a promising approach in the improvement of laser induced lithotripsy. This can be extrapolated from Fig. 5 and Fig. 6, using repetition rates of 10 Hz (Fig. 5) the shortest settings regarding to t_{total} ranged between 200 s (1J/pulse, 1 ms, 10 Hz) and 260 s (1J/pulse, 1.6 ms, 10 Hz), whereas in Fig. 6 fastest t_{total} lay between 115 s (setting 7: 1.0J/pulse, 1.2ms, 40Hz) and 150 s (setting 8: 0.5J/pulse, 0.4 ms, 80 Hz). The dusting ratios varied between 61% and 84% in all cases.

Doubling of the energy per pulse for constant pulse duration and repetition rate as mentioned beforehand (setting 1: 0.5J/pulse, 2.2 ms, 30 Hz; setting 5: 1.0J/pulse, 2.2 ms, 30 Hz) and (setting 2: 0.5 J/pulse, 1.2 ms, 40 Hz; setting 7: 1.0 J/pulse, 1.2 ms, 40 Hz) results in significant reduction of $t_{total,}$ but not in the same way for t_{break}. Even though a setting using low energy per pulse and short pulse length at high repetition rates (Fig. 6: setting 8: 0.5J/pulse, 0.4 ms, 80 Hz) was effective regarding to $t_{total,}$ but a short break up time thenceforward the remaining fragments are further crushed due to recently described "popcorn-technique" [31, 32]. There was also no improvement in t_{total} using setting 8 until t_{break} in combination with setting 4 (2.5J, 4.0 ms, 10 Hz) for continuing the treatment of the fragments. Unfortunately the experimental laser system was just available to test the settings presented, therefore it would be of interest to test such "combined settings" on significant impact on the improvement of the overall efficacy of the treatment. The correlation between the laser parameters, fragmentation times and dusting efficacy has to be further investigated, particularly in combination with the generated propulsion. Based on these first preliminary data sets in this work it will be possible to continue on profound data. Recently another potential method was published which uses experimental data on fragmentation (here: ablation volume) and propulsion at different laser settings (here: pulse duration and number of pulses, for constant pulse energy) to derive an analytic model function for predicting treatment efficacy from laser parameters [30]. This might be an interesting tool for further optimization of laser settings and laser development.

In the propulsion experiments [22], the result reproducibility was better when using spherical (first used in this work) instead of cubical stone phantoms. In Fig. 3 it is illustrated that the movement profile of the spherical stones (lower graph) during laser application is more uniform compared to that of the cubical stones (upper graph). In former experiments using cubes it was observed that the cubes became sometimes stuck in the experimental apparatus, hence the movement profile was more irregular compared to the spherical phantoms. Obviously this renders such experiments time-consuming and the result quality less satisfactory or both, which is why spherical artificial stones were introduced in this work to improve the overall quality of the set-up. In Fig. 7, most results obtained for the propulsion velocity are nevertheless in agreement for both phantom shapes. In other respects, further optimisation of the propulsion set-up might be useful in terms of adjustments to fibre distance and water flow. The experimental set-ups for fragmentation and propulsion experiments were developed on the one hand to mimic a clinical situation, but also to guarantee reproducible and reliable results in lab tests, therefore the both set-ups were optimized for good handling (Operator) and accessibility (laser fiber, maintenance). The main focus lay on the reproducible comparison of different laser settings and laser systems. Especially in case of the Propulsion set-up the vertical movement of the stone was used for evaluation was used as the gravitation served as "constant" counterforce to bring the stone back into its origin position. By keeping the water flow and level constant it was possible to achieve very similar conditions for each stone respectively laser setting tested. Even though the clinical situation differs from these experimental set-ups, the experimental procedure was in case of the

Biomedical Optics EXPRESS

propulsion experiment independent of the investigator, using the fragmentation set-up the influence of the operator (subjective influences, including motivation and experience, on the obtained results and conclusions) could successively be minimized [15]. As a consequence, a high reproducibility could gradually be achieved in the evaluation of different laser systems and laser parameters.

Besides fragmentation and movement of calculi, the fluorescence of human kidney stones was investigated in this study. Interesting approaches in this area were recently introduced that involved fluorescence excitation on kidney stones with the aiming beam of a laser system [24, 25]. This enables one to develop a feedback system for the laser device to differentiate hard and soft tissue in front of the fiber tip and finally to avoid accidental laser pulse application to surrounding soft tissue [33]. In this study it could be shown that the urinary stones emitted sufficiently intense fluorescence light, allowing to clearly distinguishing them from surrounding tissue or operation tools such as guide wires, catheters and endoscopes. With that, an endoscope-based safety feature can be envisioned in combination with a suitable color tracking algorithm. In case of the stone or the fiber out of sight or for instance inside the working channel there is a risk to hit operation tools, which could be avoided by activation of an emergency alarm [34]. Innovations in laser development resulted in the introduction of high power Ho:YAG lasers on the market, providing an average power around 100W, which can be very efficient in stone destruction [35–37]. Furthermore, attention should in particular also be dedicated to heat generation inside the urinary tract when using such high power laser devices [38–42]. Fluorescence-assisted endoscopic laser lithotripsy should be introduced in particular in connection with high power laser devices. While these may be equipped with temperature measurement features to minimize possible heat-induced damages to surrounding soft tissue, fluorescence may provide a prompter feedback signal to prevent direct laser application on tissue. Further investigations on all efficacy and safety aspects of lithotripsy (fragmentation, dusting, propulsion, stone recognition, and stone/tissue differentiation) should certainly be performed to improve the clinical outcome for the benefit of the patient.

5. Conclusion

Based on the set-ups used in this study, reproducible data sets concerning fragmentation for a variation of energy per pulse (0.5J-2.5J), pulse length (0.25 ms-4.0ms) and repetition rates (10Hz- 80Hz) were created. Elongation of pulse length (>1ms) in combination with simultaneously increase of energy per pulse dependent on the laser system's capacity and higher repetition rates (>30 Hz) seems to be a promising approach to improve fragmentation efficacy. Propulsion experiments were performed for different energies per pulse (0.5J-2.5J), pulse length (0.3ms, 0.6ms, 1.0ms) at repetition rates of 10 Hz showing that the reproducibility of the results could be improved by the use of spherical instead of cubical artificial stones. In combination these data sets can be used to obtain laser lithotripsy procedure, meaning using the full potential (high ablation rate, smallest fragment diameter (dust), lowest propulsion) of laser devices currently or in the future available on the market. Broadband fluorescence response of human calculi could be a useful tool to retrieve lost stones or fragments (possible increase of stone free rate) or can be used as a further safety feature for laser lithotripsy (reduction of collateral damage to surrounding tissue or endoscopic devices).

Acknowledgments

This manuscript is part of the inaugural thesis of Maximilian Eisel to be submitted at the Medical Faculty of the Ludwig-Maximilians-Universität, Munich.

Disclosures

The authors declare that there are no conflicts of interest related to this article.

Biomedical Optics EXPRESS

References

1. M. T. Gettman and J. W. Segura, "Management of ureteric stones: issues and controversies," BJU Int. **95**(s2), 85–93 (2005).
2. S. P. Dretler, "Laser lithotripsy: a review of 20 years of research and clinical applications," Lasers Surg. Med. **8**(4), 341–356 (1988).
3. A. Hofstetter, "Lasers in urology," Lasers Surg. Med. **6**(4), 412–414 (1986).
4. A. Vogel, "Nonlinear absorption: intraocular microsurgery and laser lithotripsy," Phys. Med. Biol. **42**(5), 895–912 (1997).
5. B. Altay, B. Erkurt, and S. Albayrak, "A review study to evaluate holmium:YAG laser lithotripsy with flexible ureteroscopy in patients on ongoing oral anticoagulant therapy," Lasers Med. Sci. **32**(7), 1615–1619 (2017).
6. A. Hofstetter, "The Laser in Urology (State of the Art)," Laser-Medizin **15**(4), 155–160 (2000).
7. A. J. Marks, J. Qiu, T. E. Milner, K. F. Chan, and J. M. H. Teichman, "Laser lithotripsy physics," in *Urinary Tract Stone Disease*, N. P. Rao, G.M. Preminger, and J. P. Kavanagh, eds. (Springer, 2011), pp. 301–309.
8. R. Sroka, T. Pongratz, F. Strittmatter, M. Eisel, and S. Ströbl, "In-vitro investigation on fragmentation/dusting and fluorescence during Ho:YAG-Laser induced lithotripsy," (Conference Presentation) in *SPIE BiOS* (SPIE, 2018).
9. H. Lee, R. T. Ryan, J. M. H. Teichman, J. Kim, B. Choi, N. V. Arakeri, and A. J. Welch, "Stone retropulsion during holmium:YAG lithotripsy," J. Urol. **169**(3), 881–885 (2003).
10. M. Sofer, J. D. Watterson, T. A. Wollin, L. Nott, H. Razvi, and J. D. Denstedt, "Holmium:YAG laser lithotripsy for upper urinary tract calculi in 598 patients," J. Urol. **167**(1), 31–34 (2002).
11. H. W. Kang, H. Lee, J. M. H. Teichman, J. Oh, J. Kim, and A. J. Welch, "Dependence of calculus retropulsion on pulse duration during Ho: YAG laser lithotripsy," Lasers Surg. Med. **38**(8), 762–772 (2006).
12. J. Sea, L. M. Jonat, B. H. Chew, J. Qiu, B. Wang, J. Hoopman, T. Milner, and J. M. Teichman, "Optimal power settings for Holmium:YAG lithotripsy," J. Urol. **187**(3), 914–919 (2012).
13. M. M. Elhilali, S. Badaan, A. Ibrahim, and S. Andonian, "Use of the Moses Technology to Improve Holmium Laser Lithotripsy Outcomes: A Preclinical Study," J. Endourol. **31**(6), 598–604 (2017).
14. P. Kronenberg and O. Traxer, "In vitro fragmentation efficiency of holmium: yttrium-aluminum-garnet (YAG) laser lithotripsy--a comprehensive study encompassing different frequencies, pulse energies, total power levels and laser fibre diameters," BJU Int. **114**(2), 261–267 (2014).
15. M. J. Bader, T. Pongratz, W. Khoder, C. G. Stief, T. Herrmann, U. Nagele, and R. Sroka, "Impact of pulse duration on Ho:YAG laser lithotripsy: fragmentation and dusting performance," World J. Urol. **33**(4), 471–477 (2015).
16. S. P. Dretler, "Ureteroscopy for Proximal Ureteral Calculi: Prevention of Stone Migration," J. Endourol. **14**(7), 565–567 (2000).
17. R. Sroka, T. Pongratz, G. Scheib, W. Khoder, C. G. Stief, T. Herrmann, U. Nagele, and M. J. Bader, "Impact of pulse duration on Ho:YAG laser lithotripsy: treatment aspects on the single-pulse level," World J. Urol. **33**(4), 479–485 (2015).
18. P. Kronenberg and O. Traxer, "Update on lasers in urology 2014: current assessment on holmium:yttrium-aluminum-garnet (Ho:YAG) laser lithotripter settings and laser fibers," World J. Urol. **33**(4), 463–469 (2015).
19. T. C. Hutchens, D. A. Gonzalez, P. B. Irby, and N. M. Fried, "Fiber optic muzzle brake tip for reducing fiber burnback and stone retropulsion during thulium fiber laser lithotripsy," J. Biomed. Opt. **22**(1), 018001 (2017).
20. R. Sroka, N. Haseke, T. Pongratz, V. Hecht, D. Tilki, C. G. Stief, and M. J. Bader, "In vitro investigations of repulsion during laser lithotripsy using a pendulum set-up," Lasers Med. Sci. **27**(3), 637–643 (2012).
21. J. J. Zhang, D. Rajabhandharaks, J. R. Xuan, R. W. J. Chia, and T. Hasenberg, "Calculus migration characterization during Ho:YAG laser lithotripsy by high-speed camera using suspended pendulum method," Lasers Med. Sci. **32**(5), 1017–1021 (2017).
22. M. Eisel, S. Ströbl, T. Pongratz, F. Strittmatter, and R. Sroka, "In vitro investigations of propulsion during laser lithotripsy using video tracking," Lasers Surg. Med. **50**(4), 333–339 (2018).
23. D. Schlager, J. Schütz, A. Brandenburg, and A. Miernik, "1201 - Seek and destroy: A novel laser system with real-time automatic target identification for urinary stone lithotripsy. An in-vivo study," Eur. Urol. Suppl. **17**(2), e1682 (2018).
24. B. Lange, J. Cordes, and R. Brinkmann, "Stone/tissue differentiation for holmium laser lithotripsy using autofluorescence," Lasers Surg. Med. **47**(9), 737–744 (2015).
25. B. Lange, D. Jocham, R. Brinkmann, and J. Cordes, "Stone/tissue differentiation for Holmium laser lithotripsy using autofluorescence: clinical proof of concept study," Lasers Surg. Med. **49**(4), 361–365 (2017).
26. K. Stock, D. Steigenhöfer, T. Pongratz, R. Graser, and R. Sroka, "Investigation on cavitation bubble dynamics induced by clinically available Ho:YAG lasers," Photonics Lasers Med. **5**(2), 141–6150 (2016).
27. R. Li, D. Ruckle, M. Keheila, J. Maldonado, M. Lightfoot, M. Alsyouf, A. Yeo, S. R. Abourbih, G. Olgin, J. L. Arenas, and D. D. Baldwin, "High-frequency dusting versus conventional holmium laser lithotripsy for intrarenal and ureteral calculi," J. Endourol. **31**(3), 272–277 (2017).
28. D. A. Wollin, E. C. Carlos, W. R. Tom, W. N. Simmons, G. M. Preminger, and M. E. Lipkin, "Effect of laser settings and irrigation rates on ureteral temperature during holmium laser lithotripsy, an in vitro model," J. Endourol. **32**(1), 59–63 (2018).

Biomedical Optics EXPRESS

29. E. Esch, W. N. Simmons, G. Sankin, H. F. Cocks, G. M. Preminger, and P. Zhong, "A simple method for fabricating artificial kidney stones of different physical properties," Urol. Res. **38**(4), 315–319 (2010).
30. D. A. Rebuck, A. Macejko, V. Bhalani, P. Ramos, and R. B. Nadler, "The natural history of renal stone fragments following ureteroscopy," Urology **77**(3), 564–568 (2011).
31. P. Klaver, T. de Boorder, A. I. Rem, T. M. T. W. Lock, and H. J. Noordmans, "In vitro comparison of renal stone laser treatment using fragmentation and popcorn technique," Lasers Surg. Med. **49**(7), 698–704 (2017).
32. A. H. Aldoukhi, W. W. Roberts, T. L. Hall, and K. R. Ghani, "Holmium laser lithotripsy in the new stone age: dust or bust?," Frontiers in Surgery **4**, 57 (2017).
33. D. Beaucamp, R. Engelhardt, P. Hering, and W. Meyer, *Stone Identification during Laser Induced Shock Wave Lithotripsy* (Springer Berlin Heidelberg, 1990).
34. K. Xavier, G. W. Hruby, C. R. Kelly, J. Landman, and M. Gupta, "Clinical evaluation of efficacy of novel optically activated digital endoscope protection system against laser energy damage," Urology **73**(1), 37–40 (2009).
35. M. S. Nomikos, G. Koritsiadis, N. Bafaloukas, G. Athanasopoulos, and S. Papanikolaou, "P10 - Safety and efficacy of high power Holmium-Yag laser in percutaneous nephrolithotomy," Eur. Urol. Suppl. **17**(4), e2017 (2018).
36. J. W. Lee, J. Park, M. C. Cho, H. Jeong, H. Son, and S. Y. Cho, "PD30-12 How to perform the dusting technique for calcium oxalate stones during Ho:YAG lithotripsy," J. Urol. **197**(4), 582 (2017).
37. S. Chen, L. Zhu, S. Yang, W. Wu, L. Liao, and J. Tan, "High- vs low-power holmium laser lithotripsy: a prospective, randomized study in patients undergoing multitract minipercutaneous nephrolithotomy," Urology **79**(2), 293–297 (2012).
38. S. Hein, R. Petzold, M. Schoenthaler, U. Wetterauer, and A. Miernik, "Thermal effects of Ho: YAG laser lithotripsy: real-time evaluation in an in vitro model," World J. Urol. **36**(9), 1469–1475 (2018).
39. D. A. Wollin, E. C. Carlos, W. R. Tom, W. N. Simmons, G. M. Preminger, and M. E. Lipkin, "Effect of laser settings and irrigation rates on ureteral temperature during holmium laser lithotripsy, an in vitro model," J. Endourol. **32**(1), 59–63 (2018).
40. A. H. Aldoukhi, K. R. Ghani, T. L. Hall, and W. W. Roberts, "Thermal response to high-power holmium laser lithotripsy," J. Endourol. **31**(12), 1308–1312 (2017).
41. A. H. Aldoukhi, T. L. Hall, K. R. Ghani, A. D. Maxwell, B. MacConaghy, and W. W. Roberts, "Caliceal fluid temperature during high-power holmium laser lithotripsy in an in vivo porcine model," J. Endourol. **32**(8), 724–729 (2018).
42. W. R. Molina, I. N. Silva, R. Donalisio da Silva, D. Gustafson, D. Sehrt, and F. J. Kim, "Influence of saline on temperature profile of laser lithotripsy activation," J. Endourol. **29**(2), 235–239 (2015).

138.246.2.190 {ts '2019-11-20 05:31:21'}